NANO LETTERS
Cite This: Nano Lett. XXXX, XXX, XXX−XXX
Letter
pubs.acs.org/NanoLett

Ultrabright Room-Temperature Sub-Nanosecond Emission from Single Nitrogen-Vacancy Centers Coupled to Nanopatch Antennas

Simeon I. Bogdanov,*[,†,‡] Mikhail Y. Shalaginov,[†,‡] Alexei S. Lagutchev,[†,‡] Chin-Cheng Chiang,[†,‡] Deesha Shah,[†,‡] Alexandr S. Baburin,[§,∥] Ilya A. Ryzhikov,[§,⊥] Ilya A. Rodionov,[§,∥] Alexander V. Kildishev,[†,‡] Alexandra Boltasseva,[†,‡] and Vladimir M. Shalaev[†,‡]

[†]School of Electrical & Computer Engineering and Birck Nanotechnology Center, Purdue University, West Lafayette, Indiana 47907, United States
[‡]Purdue Quantum Center, Purdue University, West Lafayette, Indiana 47907, United States
[§]FMNS REC, Bauman Moscow State Technical University, Moscow 105005, Russia
[∥]Dukhov Research Institute of Automatics, Moscow 127055, Russia
[⊥]Institute for Theoretical and Applied Electromagnetics RAS, Moscow 125412, Russia

Supporting Information

ABSTRACT: Solid-state quantum emitters are in high demand for emerging technologies such as advanced sensing and quantum information processing. Generally, these emitters are not sufficiently bright for practical applications, and a promising solution consists in coupling them to plasmonic nanostructures. Plasmonic nanostructures support broadband modes, making it possible to speed up the fluorescence emission in room-temperature emitters by several orders of magnitude. However, one has not yet achieved such a fluorescence lifetime shortening without a substantial loss in emission efficiency, largely because of strong absorption in metals and emitter bleaching. Here, we demonstrate ultrabright single-photon emission from photostable nitrogen-vacancy (NV) centers in nanodiamonds coupled to plasmonic nanocavities made of low-loss single-crystalline silver. We observe a 70-fold difference between the average fluorescence lifetimes and a 90-fold increase in the average detected saturated intensity. The nanocavity-coupled NVs produce up to 35 million photon counts per second, several times more than the previously reported rates from room-temperature quantum emitters.

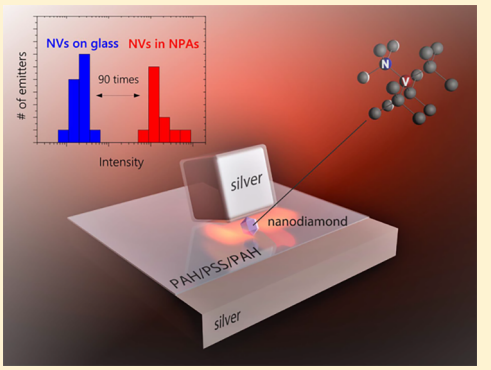

KEYWORDS: *Quantum plasmonics, nitrogen-vacancy centers, single-photon source, nanodiamonds, nanopatch antennas, epitaxial silver*

Single-photon emitters,[1] such as single molecules, quantum dots, color centers in crystals, or rare-earth atoms, are of great interest for applications in quantum information processing,[2] quantum chemistry,[3] and biology.[4] These quantum sources emit light with unique properties including antibunching, absence of ensemble broadening, extreme sensitivity to the local environment, and, in some cases, photon indistinguishability.[5−8] These emitters are usually very dim, making it challenging to harness their emission.

Typical detected photon rates from bare quantum emitters are in the range from 10^4 to 10^5 counts per second (cps),[1] only rarely exceeding 10^6 cps.[9−11] The most fundamental limiting factors for the detected photon rate from quantum emitters are radiative lifetime and photon collection efficiency. By solely increasing the collection efficiency,[12−17] detected photon rates from single emitters can exceed 10^6 cps.[16,17] Another approach for brightness enhancement hinges on drastically increasing the local density of states (LDOS) in the vicinity of the emitter, leading to a faster photon emission.[18] Dielectric[19−21] and plasmonic[22] resonators are typically used for LDOS enhancement, with alternative approaches relying on slow light[23,24] and metamaterial dispersion.[25,26]

The local density of states is proportional to the ratio of the resonance quality factor to the volume where the field is localized. In accord with this, LDOS enhancement is typically achieved by using either highly resonant but relatively large (diffraction-limited) dielectric structures or plasmonic nanostructures with lower resonance quality factors but smaller, subdiffraction size volumes. Dielectric resonators and slow light waveguides enhance the LDOS by increasing the interaction time between the dipole and the emitted field. However, as the quality factor Q of the dielectric structure increases, the long photon storage time becomes an impedi-

Received: April 9, 2018
Revised: June 22, 2018
Published: July 3, 2018

DOI: 10.1021/acs.nanolett.8b01415
Nano Lett. XXXX, XXX, XXX−XXX

ment to faster emission and limits the lifetime shortening.[27] Alternatively, plasmonic nanostructures ensure broadband (i.e., low-Q) LDOS enhancement, and their theoretical potential for lifetime shortening is about 2 orders of magnitude higher.[28] The shortcoming of plasmonic nanostructures is the high loss resulting from nonradiative quenching of excitation and plasmon absorption in metals.

Nanostructures with gap−surface−plasmon or metal−insulator−metal (MIM) modes alleviate the quenching problem. Despite their proximity to the metal, the coupling rate of the emitter to the gap-plasmonic mode is comparable to the quenching rate even as the gap shrinks below 10 nm.[29,30] Furthermore, forming a gap-plasmon resonator by replacing the top metal layer with a nanoparticle results in a nanopatch antenna (NPA) geometry.[31] The NPAs radiate electromagnetic energy on a time scale comparable to the plasmon lifetime,[32] which mitigates plasmon absorption. Still, thanks to nanosized gaps, the concentration of the electromagnetic field in NPAs is sufficient to observe strong emitter−plasmon coupling at room temperature.[33] As a result, NPAs are emerging as the systems of choice for enhancing the brightness of nanoscale emitters.[34,35] Impressive results of single-photon emission in NPAs have been recently demonstrated using colloidal quantum dots with a strong lifetime shortening, antibunching photon statistics, and photon counts exceeding 1 Mcps.[36] Nevertheless, due to photobleaching of quantum dots used in that experiment, it was not possible to reach the saturation regime and assess the emitter efficiency. The full potential of quantum emitter brightness enhancement by plasmonic nanoantennas still remains to be realized.

To overcome the problem of photostability and reduce plasmonic losses, in this work, we use a nitrogen-vacancy (NV) center[37] in a nanodiamond coupled to an all-crystalline-silver NPA (see Figure 1). The photostability of NV centers combined with an ultralow loss of the silver film ($\varepsilon'' = 0.11$ at 650 nm, see the Supporting Information, section I) leads to detected brightness in the range of tens of Mcps. By observing fluorescence saturation and radiation patterns, we were able to quantify the factors leading to the brightness enhancement.

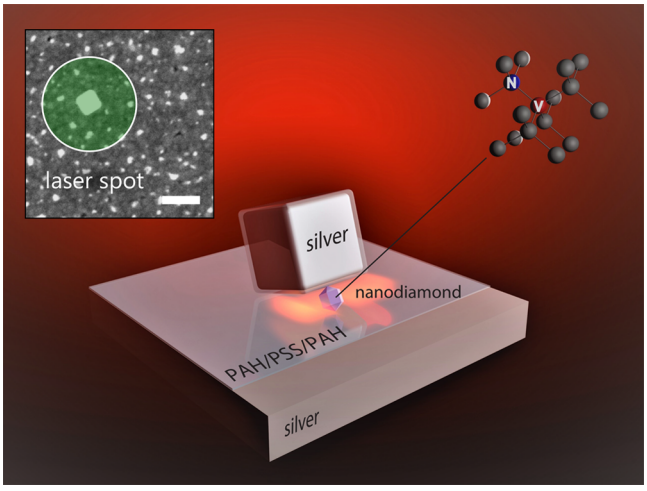

Figure 1. Schematic view of an all-silver nanopatch antenna (NPA) structure. A silver nanocube is deposited on silver substrate, with a nanodiamond, containing a nitrogen-vacancy (NV) center, placed in between. The inset shows an SEM micrograph of the Ag substrate with randomly dispersed nanodiamonds and a 100 nm Ag nanocube. The scale bar is 200 nm. The green circle schematically shows the focused laser beam spot used for optical excitation.

Results. *Sample Design and Fabrication.* In our experiment, the NVs were hosted by nanodiamonds with a diameter of $d_{ND} = 20 \pm 5$ nm, where each nanodiamond nominally contained 1−2 NVs. Two main samples were used in the study: one sample containing nanodiamonds with NVs coupled to NPAs and a bare glass coverslip substrate with dispersed nanodiamonds. The sample with NPAs was fabricated according to the procedure well documented in prior works.[31,36,38] We deposited a 35 nm thin low-loss, epitaxial silver and an approximately 6 nm thick dielectric spacer. The latter was formed using layer-by-layer alternate deposition of poly(allyalamine hydrochloride) (PAH) and polystyrenesulfonate (PSS). Nanodiamonds and subsequently 100 nm size single-crystalline nanocubes were randomly dispersed on the spacer layer. This step resulted in the random formation of NPAs with NV centers inside (see inset of Figure 1). To highlight the role of an epitaxial substrate, a similar sample was made using polycrystalline silver. We found that the polycrystalline sample exhibits at least 5 times higher losses than the epitaxial film at the wavelengths of interest (see discussion below and Figure S5). The control sample was fabricated by randomly dispersing the nanodiamonds on a glass coverslip substrate with refractive index $n = 1.525$. In the control experiment, we measured the photophysical characteristics of 14 single NV centers.

Single-Emitter Characterization. We selected the brightest emitter from both the NPA-enhanced set and the control set (see the Supporting Information, section IV) and compared their photophysical properties. From now on, these emitters are referred to as NV-NPA and NV-G, respectively. The NV-NPA emitter was analyzed using an air objective with a numerical aperture of 0.9. Antibunching behavior was characterized by the second order autocorrelation function $g^{(2)}_{\text{NV-NPA}}(t)$ measured under continuous excitation. The fitting of the autocorrelation function accounted for the finite time resolution of the Hanbury-Brown−Twiss setup measured at 263 ± 8 ps (see the Methods section). The extracted value of $g^{(2)}_{\text{NV-NPA}}(0) = 0.41 \pm 0.03$ points toward the presence of a single NV inside the NPA (Figure 2a). Background emission from the planar silver film was found negligible and not likely to significantly contribute to $g^{(2)}_{\text{NV-NPA}}(0)$. $g^{(2)}_{\text{NV-NPA}}(0)$ is likely limited either by an ultrafast component of the NV emission or by background emission from the NPA site. Using pulsed excitation, we characterized the fluorescence lifetime by measuring the fluorescence decay (Figure 2b). The NV-NPA fluorescence decay consists of two components with characteristic times $\tau_1 = 30 \pm 20$ ps and $\tau_2 = 360 \pm 30$ ps. These time constants were determined by convolution of the sum of two exponential decays with the instrument response function (IRF) having a full width half-maximum of 96 ps. The slower component is attributed to the NV emission, as τ_2 is consistent with the emission rate obtained from simulation (see the Supporting Information, section III), as well as with the value extracted from the autocorrelation measurement. The antibunching of the faster decay component cannot be measured in our experimental setting. Therefore, it cannot be safely attributed to the NV emission and instead may be due to the light produced by either the metal nanostructure[39] or the polymer layers.

Next, we analyzed the emitter brightness. The fluorescence saturation curve was background corrected using the

DOI: 10.1021/acs.nanolett.8b01415
Nano Lett. XXXX, XXX, XXX−XXX

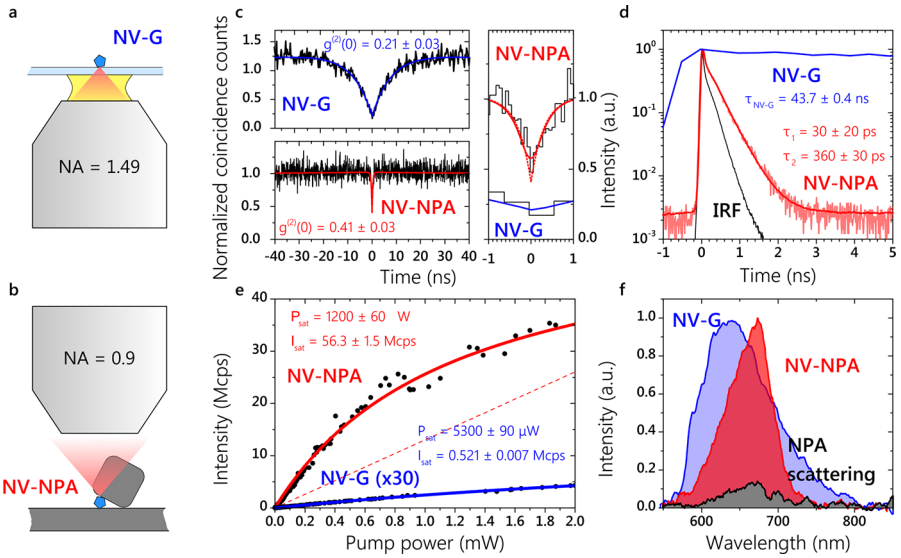

Figure 2. Schematic illustration of the collection configurations used for the NV center in a nanodiamond on a coverslip glass substrate (NV-G, a) and the NV coupled to a nanopatch antenna (NV-NPA, b).Photophysical characterization of NV-G (blue) and NV-NPA (red), including (c) autocorrelation curves, (d) fluorescence decay curves, (e) saturation curves, and (f) emission and scattering spectra. Both the convoluted (solid red) and deconvoluted (dotted red) fits are shown for the antibunching curve of the NV-NPA. The IRF curve in part b describes the instrument response function. The fluorescence decay curve of the NV-NPA (light pink) is fitted (red) using a sum of two exponential decays with time constants τ_1 and τ_2 convoluted with the IRF. The decay curve of the NV-G in part b is fitted with a single-exponential function. The saturation curve of the NV-NPA has been corrected by subtracting the background component (dashed red).

autocorrelation data. The fraction of the emission due to the background in the linear regime r_{bg} has been calculated as $r_{bg} = 1 - \sqrt{1 - g^{(2)}(0)}$.[16] The linear background component plotted in Figure 2c with the red dashed line has been subtracted from the raw saturation data. This linear component possibly originated from the same source as the fast component of the fluorescence decay. The remaining saturable component (red curve) yields $I^{sat}_{NV\text{-}NVA} = 56.3 \pm 1.5$ Mcps. The saturating laser power (measured before coupling to the objective) was $P^{sat}_{NV\text{-}NVA} = 1.20 \pm 0.06$ mW. In Figure 2d, we compare the spectra of nanoantenna scattering and NV-NPA emission. The dark field scattering spectrum from NV-NPA overlaps well with the photoluminescence spectrum of the coupled emitter. We conclude that the enhanced emission indeed resulted from coupling of the NV to the mode of the NPA.

The NV-G source was analyzed using an oil immersion objective with numerical aperture (NA) = 1.49 in the total internal reflection mode. The photon purity was characterized by an autocorrelation at zero delay of $g^{(2)}_{NV\text{-}G}(0) = 0.21 \pm 0.03$, limited by the background fluorescence from the coverslip glass. The measured fluorescence lifetime was $\tau_{NV\text{-}G} = 43.7 \pm 0.4$ ns, which is over 120 times longer than in the case of the NV-NPA. We extract the saturated intensity of $I^{sat}_{NV\text{-}G} = 520 \pm 7$ kcps, over 100 times weaker than for NV-NPA. The saturating laser power of $P^{sat}_{NV\text{-}G} = 5.3 \pm 0.09$ mW is of the same order as that of NV-NPA. The photoluminescence spectrum of NV-G plotted on Figure 2d extends from 570 to 780 nm and indicates that both charge states NV^0 and NV^- likely contribute to the emission.[40]

We now statistically compare the results from the coverslip and NPA-enhanced NV sets (see Figure 3), where the data were collected for 14 and 11 emitters, respectively. The average lifetime shortening of 70 times was observed between the sets of NVs on coverslip and NPA-enhanced NVs (0.93 vs

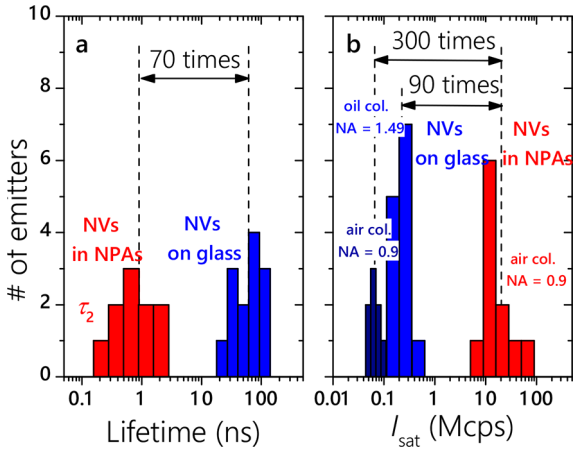

Figure 3. Statistical comparison between the sets of NVs on glass coverslip and NPA-enhanced NVs in terms of (a) lifetime shortening and (b) saturated brightness enhancement.

62 ns). The fluorescence lifetime for NPA-enhanced NVs is remarkably shorter compared to what has been previously observed for NVs in small nanodiamonds or near the diamond−air interface, which typically exhibit fluorescence lifetimes in excess of 10 ns.[41,42] NVs in nanodiamonds have also been reported to suffer from low quantum efficiency,[43] which impedes fluorescence lifetime shortening. So far, despite the implementation of both photonic and plasmonic LDOS enhancement techniques, the emission lifetimes obtained with NVs have failed to fall below 1 ns. In our experiment, large broadband LDOS and high outcoupling efficiency of NPAs resulted in ultrabright antibunched emitters with sub-nanosecond fluorescence lifetimes. The average lifetime shortening due to NPAs of 70 times can be compared to the numerically simulated lifetime shortening of roughly 220 (in the case of a vertically oriented emission dipole embedded into a 15 nm

DOI: 10.1021/acs.nanolett.8b01415
Nano Lett. XXXX, XXX, XXX−XXX

Table 1. Comparative Summary of the Average Photophysical Quantities between NPA-Enhanced NVs and NVs on Coverslip: Total Decay Rate γ^{tot}, Emission Intensity at Saturation I^{sat}, and the Saturating Laser Power P^{sat}

	γ^{tot} (ns^{-1})	I^{sat} (Mcps)	P^{sat} (mW)
NVs in NPAs	$(0.93 \pm 0.81)^{-1}$	20 ± 17 (NA = 0.9)	0.62 ± 0.37
NVs on coverslip	$(62 \pm 33)^{-1}$	0.22 ± 0.11 (oil col. NA = 1.49); 0.066 ± 0.017 (air col. NA = 0.9)	1.4 ± 1.2
ratio	70	90 (oil col. NA = 1.49); 300 (air col. NA = 0.9)	0.45

diameter spherical nanodiamond). The discrepancy between the two values can be attributed to an imperfect spectral overlap between the cavity and NV radiation spectrum, a misalignment between the dipole orientation and local electric field of the cavity mode and nonunity quantum yield of NVs in nanodiamonds.

The average saturated brightness is 90 times higher on average in NPA-enhanced NVs than for the NVs on coverslip, which were analyzed using an oil objective with NA = 1.49 (20 vs 0.22 Mcps, see Figure 3b). We note that the fluorescence lifetime characteristics of the NPA-enhanced emitters on the polycrystalline-silver substrate are comparable to those observed with epitaxial silver. However, due to higher losses of the polycrystalline silver, the saturated emission was on average several times weaker than that on epitaxial silver substrate (2.8 vs 20.0 Mcps). The characterization data for several additional NPA-enhanced emitters on epitaxial and polycrystalline-silver substrates are shown in Figures S4 and S5, respectively. Furthermore, we characterized saturated intensity for 8 NVs on coverslip using an air objective with NA = 0.9, with access from the air side, and found 0.066 Mcps on average. For those NVs, autocorrelation was not verified, so this number represents an upper bound on the average saturated intensity for single NVs. Compared to NVs on coverslip analyzed with the air objective, the NPA-enhanced set presents an average increase in brightness of 300 times. Table 1 summarizes the average photophysical properties of the NV sets.

Despite a drastic lifetime shortening compared to the set of NVs on coverslip, the emission of NPA-enhanced NVs is saturated at a comparable excitation laser power. One can conclude that the excitation rate at constant pump power is also strongly enhanced by the NPA. By comparing the average specific excitation rates $c^{exc} = \gamma^{tot}/P^{sat}$ between the coverslip and NPA-enhanced NV sets, and accounting for the difference between numerical apertures used for pump delivery in both experiments, we find an increase in NV absorption cross-section of 200 times due to the NPA. The enhancement of both emission and absorption is a consequence of multiple broad resonances present in NPAs.[44] It was previously shown that, at high incident pump powers, the properties of the optical modes in NPAs were altered due to structural deformation.[39] Strong local enhancement of pump intensity in NPAs allows to obtain the same excitation rate at a reduced total incident pump power. Therefore, the local pump enhancement is important to guarantee a high emitter brightness without degrading the antenna properties. In the future, these resonances could be engineered[45] to precisely match the absorption and emission frequencies of narrow-band emitters, yielding an even larger intensity enhancement and better photon purity.[46]

Extraction of Emitter Efficiency. The increase in saturated brightness provided by the NPAs is commensurate with the observed lifetime shortening, suggesting that these plasmonic nanostructures are highly efficient. However, to account for the influence of different factors leading to the detected brightness enhancement, we perform a quantitative efficiency analysis. The total emitter efficiency $\eta^{tot} = I^{sat}/\gamma^{tot}$ is defined as the ratio between the detected saturated fluorescence intensity I^{sat} and the total decay rate γ^{tot}. The average total emitter efficiency was found to be almost identical between the NPA-enhanced set and the coverslip set (about 1.2% in both cases). These values depend on the efficiency parameters of the microscope setup. To obtain an instrument-independent quantity, we calculate the photon efficiency η^{ph}, i.e., the number of photons emitted into the far-field per NV excitation event. The photon efficiency can be either calculated from the assumed microscopic properties of the photon source or deduced from the observed total fluorescence intensity. We use both approaches to estimate, respectively, the upper ($\eta^{ph,sim}$) and lower ($\eta^{ph,meas}$) bounds for the photon efficiency of NPA-enhanced NVs and NVs on coverslip. These quantities are summarized in Table 2.

Table 2. Summary of NV-G and NV-NPA Measured Total Efficiency and Estimated Photon Efficiency Values

	η^{tot} (%)	$\eta^{ph,meas}$ (%)	$\eta^{ph,sim}(z)$ (%)
NVs in NPAs	1.2 ± 0.8	17 ± 11	98
NVs on coverslip	1.2 ± 0.6	11 ± 6	40 ± 20

The upper bound for photon efficiency is obtained from full-field simulations. We define the simulated photon efficiency as

$$\eta^{ph,sim} = \frac{\gamma^{ff}}{\gamma^{ff} + \gamma^{loss} + \gamma^{nr}} \quad (1)$$

where γ^{ff} is the rate of photon emission into the far-field by an NV center with unity quantum yield, γ^{loss} is the total rate of dissipation to heat consisting of quenching and plasmon absorption, and γ^{nr} is the intrinsic rate of nonradiative decay. For the case of NV on coverslip, there are no losses to the metal, so the photon efficiency is identically equal to the quantum yield and limited by γ^{nr}. For the NPA-enhanced case, the photon efficiency is, in contrast, dominated by losses to the metal, while the nonradiative rate is bound by the total measured decay rate of NVs on glass and is therefore negligible.

While calculating γ^{ff} and γ^{loss}, we first obtain the electromagnetic field distributions near the emitters, assuming an ND size of 15 nm. Figure 4a,b shows the plots of the normalized electric field intensities, with a several orders of magnitude enhancement in the near-field of the NPA. The observed average lifetime shortening of 70 times is in reasonable agreement with a 220-fold shortening obtained in the simulation. By calculating the fraction of the total emitted power that is lost in the metal layers, we estimate the photon efficiency of an NPA-enhanced NV to be $\eta^{ph,sim}_{NPA} \approx 98\%$ in the case of a vertically oriented dipole (see the Supporting Information, section III). The lower bound on γ^{nr} is obtained from the measurement of the fluorescence lifetime (see the

DOI: 10.1021/acs.nanolett.8b01415
Nano Lett. XXXX, XXX, XXX−XXX

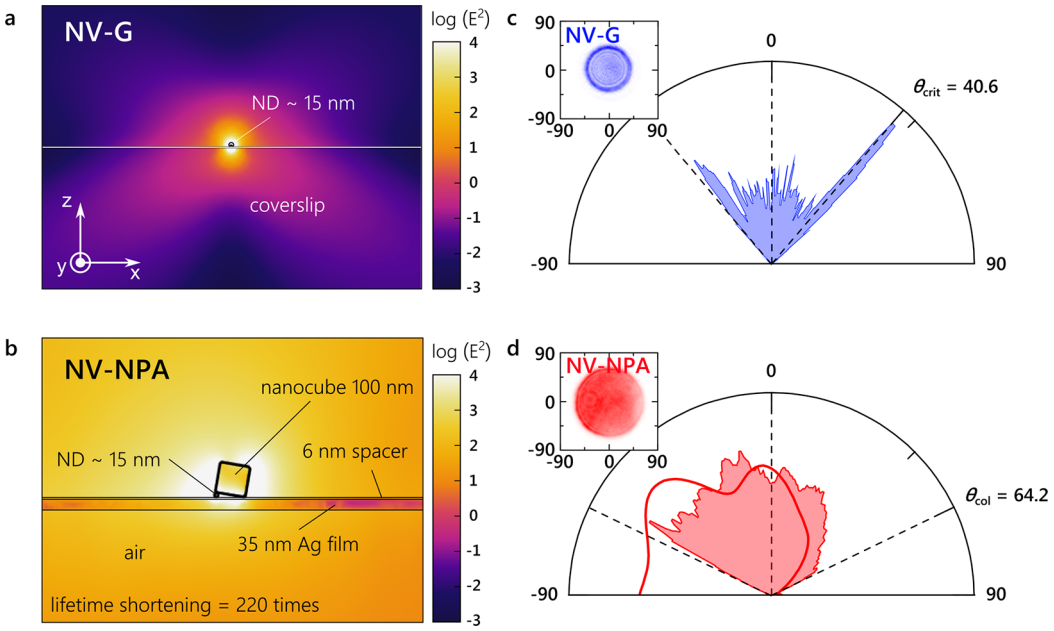

Figure 4. Near-field logarithmic electric field intensity distributions for the (a) NV-G and the (b) NV-NPA. Radiation patterns determined from back-focal plane (BFP) measurements for (c) the NV-G and (d) the NV-NPA. Red solid line in part d represents the result of a numerical simulation (see the Supporting Information, section III). Insets show the corresponding two-dimensional intensity distribution measured in the back-focal plane (BFP).

Supporting Information, section V). This estimate leads to $\eta^{ph,sim}_{glass,NA=1.49}$ 40 ± 20%.

The lower bound on the photon efficiency $\eta^{ph,meas}$ is calculated based on the measured total efficiency η^{tot} using the following relation:

$$\eta^{tot} = \eta^{ph,meas}\eta^{col,meas}\eta^{setup} \quad (2)$$

where $\eta^{col,meas}$ is the collection efficiency of the emitted photons by an objective inferred from measurement, and η^{setup} is the detection efficiency of the scanning confocal microscope, which includes the losses incurred at all the optical components and detector efficiency. $\eta^{setup} \approx 14\%$ is directly measured by using a collimated laser beam of known power at 638 nm wavelength flooding the back aperture of the objective and reflected by a mirror placed at the sample location (for more details, see the Supporting Information, section II). We assume that the oil objective (NA = 1.49) and the air objective (NA = 0.9) have the same transmission coefficient in the red region of the visible range. $\eta^{col,meas}$ is determined based on the results of the back-focal plane measurements (see insets in Figure 4c,d). The NVs on coverslip are expected to radiate mostly into the glass with an emission angular pattern concentrated around the critical angle. A simple analytical estimate predicts the fraction of the total emitted power into the glass to be 82% for the horizontal dipole and 85% for the vertical dipole (see the Supporting Information, section III). The results of this model agree reasonably well with the emission's measured angular distribution (see Figure 4c). The observed deviation from the model is most likely due to objective-induced aberrations. Therefore, we assume that the collection efficiency for NVs on coverslip is 85%. On the other hand, the emission pattern of the NPA-enhanced NVs should vary widely depending on the exact relative position of the nanodiamond and the nanocube. In the experiment, we observe an essentially nondirectional pattern within the NA = 0.9 solid angle. Assuming that the emission is roughly isotropic in the upper half space, we estimate $\eta^{col,meas} \approx 50\%$. With these numbers, we estimate the average lower-bound photon efficiencies at $\langle\eta^{ph,meas}_{glass,NA=1.49}\rangle$ = 11% and $\langle\eta^{ph,meas}_{NPA}\rangle$ = 17%. Correspondingly, the NPA-enhanced NVs are emitting on average $\langle\eta^{ph,meas}_{NPA}/\tau_2\rangle$ = 240 million photons per second into the far-field at saturation (versus 2 million photons per second for NVs on coverslip). The fact that both the enhanced emitter set and the control set exhibit similar average photon efficiencies and average total efficiencies leads to the conclusion that the brightness enhancement in these nanocavities is mostly due to the strong lifetime shortening.

Discussion. When it comes to enhancing quantum emitters' performance, the approaches based on plasmonic nanocavities often suffer from a trade-off between lifetime shortening and emitter efficiency. This work demonstrates that nanopatch antennas can shorten quantum emitter lifetime by almost 2 orders of magnitude and yet preserve the efficiency of the original emitters. Because plasmonic nanocavities are more broadband than dielectric resonators at similar coupling strengths, they present a particular advantage for broadband room-temperature quantum emitters.

These results could be further improved by employing passivated epitaxial silver substrates, deterministic positioning of the nanocube with respect to the emitter,[47] and control over the emitter dipole orientation. The results show strong promise of epitaxial, all-silver NPAs for engineering ultrabright plasmon-assisted emission from single-fluorescent objects with broadband spectrum. Coupling different emitter types to similar nanogap structures may be of great interest for single-molecule spectroscopy,[48] multiphoton microscopy,[49] nano-magnetometry,[50] and photonic quantum technologies.[51] It could foster new emerging fields of ultrafast single-molecule nanoscopy,[52] spectroscopy of weak and forbidden electronic transitions,[53,54] three-dimensional single-molecule nuclear magnetic resonance,[55] and cluster state engineering.[56]

DOI: 10.1021/acs.nanolett.8b01415
Nano Lett. XXXX, XXX, XXX−XXX

Specifically, in the case of NV centers, strong enhancement of brightness by plasmonic nanoantennas could result in a sensitive single-shot readout of the electron spin at room temperature. The spin coherence time of NV centers in our nanodiamonds without coupling to the NPAs is on the order of 1 μs, probably limited by impurities inside and at the surface of the nanodiamonds. For magnetometry and quantum information applications, this coherence time can be improved through surface treatment, employing seeded nanodiamond growth and applying refocusing techniques.

Methods. *Sample Fabrication.* The coverslip sample was prepared by coating the coverslip surface with one PAH monolayer and dropcasting a diluted water solution of 20 nm nanodiamonds for 10 s (Adamas Nano) before rinsing the surface with water. Polycrystalline 50 nm silver films were deposited on Si substrate with a 10 nm Ti adhesion layer. Epitaxial silver films were 35 nm thick and deposited directly on Si substrate at the BMSTU Nanofabrication Facility (Functional Micro/Nanosystems, FMNS REC, ID 74300). Three self-assembled monolayers (PAH/PSS/PAH) were deposited by alternately dipping the samples with the silver films into the corresponding solutions for 5 min. A diluted water solution of 20 nm nanodiamonds was then dropcast onto the PAH surface. Finally, a 20× diluted water/ethanol solution of 100 nm crystalline nanocubes (Nanocomposix) was dropcast on the sample.

Characterization. All the optical characterization was performed using a custom-made scanning confocal microscope with a 50 μm pinhole based on a commercial inverted microscope body (Nikon Ti−U). The optical pumping in all the experiments except the lifetime measurement was administered by a DPSS 532 nm laser. Lifetime characterization was performed using a 514 nm fiber-coupled diode laser with a nominal 100 ps pulse width and adjustable repetition rate in the 2−80 MHz range (BDL-514-SMNi, Becker & Hickl). The excitation beam was reflected off a 550 nm long-pass dichroic mirror (DMLP550L, Thorlabs), and a 550 nm long-pass filter (FEL0550, Thorlabs) was used to filter out the remaining pump power. Two avalanche detectors with a 30 ps time resolution and 35% quantum efficiency at 650 nm (PDM, Micro-Photon Devices) were used for single-photon detection during scanning, lifetime, and autocorrelation measurements. An avalanche detector with 69% quantum efficiency at 650 nm (SPCM-AQRH, Excelitas) was used for saturation measurements. Time-correlated photon counting was performed by an acquisition card with a 4 ps internal jitter (SPC-150, Becker & Hickl). The values of $g^{(2)}(0)$ were extracted by accounting for the finite time resolution of the autocorrelation experiment $\delta t_{\mathrm{instr}} = 263 \pm 8$ ps. The measured autocorrelation was fitted by a standard two-exponential model $g^{(2)}\tau = 1 - A\exp(|\tau|/\tau_A) + B\exp(|\tau|/\tau_B)$, convoluted with a Gaussian of width $\delta t_{\mathrm{instr}}$. The fitted autocorrelation at zero delay was then taken equal to $g^{(2)}(0) = 1 - A + B$.

Simulation. All full-wave 3D electromagnetic numerical simulations were performed using finite-element frequency-domain method with a commercial software (Comsol Multiphysics, Wave Optics Module). The simulation domain was a cube with a side of 1.8 μm for NV-NPA and 2.4 μm for NV-G surrounded by a 400 nm thick perfectly matching layer. The optical emitter was modeled as an AC current density inside a 2 nm diameter sphere enclosed by a 15 nm diameter diamond shell. The emitter's wavelength was fixed at 640 nm. The emitter had a vertical dipole orientation and was placed between a 35 nm Ag layer and a Ag nanocube. The nanocube was modeled having 8 nm curvature radius at its corners and covered in 3 nm PVP layer with $n = 1.4$. One ridge of the nanocube's bottom facet was in full contact with the spacer, while the nanodiamond supported the middle of the opposite ridge of the bottom facet. The spacer layer was modeled as an isotropic dielectric with $n = 1.5$.

Simulated values in Table 2 are computed assuming a vertical dipole orientation for both emitters. Vertical dipole orientation for the NV-NPA is assumed dominant because of the relatively weak Purcell effect expected for both horizontal orientations (see Supporting Information, Section III).

■ ASSOCIATED CONTENT

Supporting Information

The Supporting Information is available free of charge on the ACS Publications website at DOI: 10.1021/acs.nanolett.8b01415.

Details about silver substrates' dielectric permittivities, spacer preparation procedure, measurement of setup efficiency, simulation of the emitters' total decay rates, loss rates and collection efficiencies, statistics of reference emitter characteristics, calculation of the quantum yield of NVs in nanodiamonds, as well as antibunching curves, fluorescence decay curves, and saturation curves for additional NPA-coupled emitters on epitaxial and polycrystalline-silver substrates (PDF)

■ AUTHOR INFORMATION

Corresponding Author

*E-mail: sbogdan@purdue.edu.

ORCID

Simeon I. Bogdanov: 0000-0001-5608-546X

Alexandra Boltasseva: 0000-0002-5988-7625

Author Contributions

S. I. Bogdanov conceived the experiment and wrote the initial draft of the paper. S. I. Bogdanov and C.-C. Chiang carried out the quantum emitter characterization. M. Y. Shalaginov and A. V. Kildishev carried out the numerical simulations. S. I. Bogdanov and A. S. Lagutchev built the experimental setup. D. Shah carried out the ellipsometry characterization of polycrystalline-silver substrates and spacer layers as well as measurements of ensemble nanocavity scattering spectra. A. S. Baburin, I. A. Ryzhikov, and I. A. Rodionov grew the epitaxial silver film. S. I. Bogdanov, A. S. Lagutchev, A. Boltasseva, and V. M. Shalaev interpreted the results. A. S. Lagutchev, M. Y. Shalaginov, D. Shah, A. Boltasseva, and V. M. Shalaev contributed to writing the paper. A. Boltasseva and V. M. Shalaev supervised the project. All authors have given approval to the final version of the manuscript.

Notes

The authors declare no competing financial interest.

■ ACKNOWLEDGMENTS

The authors acknowledge O. Makarova for the AFM measurement of polycrystalline silver RMS roughness, and I. Aharonovich, M. Mikkelsen, A. Akimov, V. Vorobyov, and S. Bolshedvorskii for useful discussions. This work was partially supported by the U.S. Department of Energy, Office of Basic Energy Sciences, Division of Materials Sciences and Engineering under Award DE-SC0017717 (S. I. Bogdanov), the

DOI: 10.1021/acs.nanolett.8b01415
Nano Lett. XXXX, XXX, XXX−XXX

National Science Foundation NSF-OP Grant DMR-1506775 (D. Shah), and the Office of Naval Research (ONR) DURIP Grant N00014-16-1-2767 (equipment grant used to purchase the scanning confocal microscope, lasers, detectors, and single-photon counting capability used in this work). A. V. Kildishev acknowledges the DARPA/DSO Extreme Optics and Imaging (EXTREME) Program, Award HR00111720032 (numerical modeling and simulations).

REFERENCES

(1) Aharonovich, I.; Englund, D.; Toth, M. *Nat. Photonics* **2016**, *10*, 631−641.
(2) O'Brien, J. L. *Science* **2007**, *318*, 1567−1570.
(3) Moerner, W. E.; Shechtman, Y.; Wang, Q. *Faraday Discuss.* **2015**, *184*, 9−36.
(4) Sydor, A. M.; Czymmek, K. J.; Puchner, E. M.; Mennella, V. *Trends Cell Biol.* **2015**, *25*, 730−748.
(5) Sipahigil, A.; Jahnke, K. D.; Rogers, L. J.; Teraji, T.; Isoya, J.; Zibrov, A. S.; Jelezko, F.; Lukin, M. D. *Phys. Rev. Lett.* **2014**, *113*, 113602.
(6) Somaschi, N.; Giesz, V.; De Santis, L.; Loredo, J. C.; Almeida, M. P.; Hornecker, G.; Portalupi, S. L.; Grange, T.; Antón, C.; Demory, J.; et al. *Nat. Photonics* **2016**, *10*, 340−345.
(7) He, Y.-M.; He, Y.; Wei, Y.-J.; Wu, D.; Atatüre, M.; Schneider, C.; Höfling, S.; Kamp, M.; Lu, C.-Y.; Pan, J.-W. *Nat. Nanotechnol.* **2013**, *8*, 213−217.
(8) Müller, K.; Fischer, K. A.; Dory, C.; Sarmiento, T.; Lagoudakis, K. G.; Rundquist, A.; Kelaita, Y. A.; Vučković, J. *Optica* **2016**, *3*, 931.
(9) Tran, T. T.; Bray, K.; Ford, M. J.; Toth, M.; Aharonovich, I. *Nat. Nanotechnol.* **2015**, *11*, 37−41.
(10) Grosso, G.; Moon, H.; Lienhard, B.; Ali, S.; Efetov, D. K.; Furchi, M. M.; Jarillo-Herrero, P.; Ford, M. J.; Aharonovich, I.; Englund, D. *Nat. Commun.* **2017**, *8*, 705.
(11) Neu, E.; Agio, M.; Becher, C. *Opt. Express* **2012**, *20*, 19956.
(12) Mouradian, S. L.; Schröder, T.; Poitras, C. B.; Li, L.; Goldstein, J.; Chen, E. H.; Walsh, M.; Cardenas, J.; Markham, M. L.; Twitchen, D. J. *Phys. Rev. X* **2015**, *5*, 31009.
(13) Babinec, T. M.; Hausmann, B. J. M.; Khan, M.; Zhang, Y.; Maze, J. R.; Hemmer, P. R.; Loncar, M. *Nat. Nanotechnol.* **2010**, *5*, 195−199.
(14) Hadden, J. P.; Harrison, J. P.; Stanley-Clarke, A. C.; Marseglia, L.; Ho, Y. L. D.; Patton, B. R.; O'Brien, J. L.; Rarity, J. G. *Appl. Phys. Lett.* **2010**, *97*, 402−406.
(15) Riedel, D.; Rohner, D.; Ganzhorn, M.; Kaldewey, T.; Appel, P.; Neu, E.; Warburton, R. J.; Maletinsky, P. *Phys. Rev. Appl.* **2014**, *2*, 1−6.
(16) Wan, N. H.; Shields, B. J.; Kim, D.; Mouradian, S.; Lienhard, B.; Walsh, M.; Bakhru, H.; Schröder, T.; Englund, D. *Nano Lett.* **2018**, *18*, 2787−2793.
(17) Momenzadeh, S. A.; Stöhr, R. J.; de Oliveira, F. F.; Brunner, A.; Denisenko, A.; Yang, S.; Reinhard, F.; Wrachtrup, J. *Nano Lett.* **2015**, *15*, 165−169.
(18) Pelton, M. *Nat. Photonics* **2015**, *9*, 427−435.
(19) Wolters, J.; Schell, A. W.; Kewes, G.; Nüsse, N.; Schoengen, M.; Döscher, H.; Hannappel, T.; Löchel, B.; Barth, M.; Benson, O. *Appl. Phys. Lett.* **2010**, *97*, 2013−2016.
(20) Riedrich-Möller, J.; Pezzagna, S.; Meijer, J.; Pauly, C.; Mücklich, F.; Markham, M.; Edmonds, A. M.; Becher, C. *Appl. Phys. Lett.* **2015**, *106*, 221103.
(21) Benedikter, J.; Kaupp, H.; Hümmer, T.; Liang, Y.; Bommer, A.; Becher, C.; Krueger, A.; Smith, J. M.; Hänsch, T. W.; Hunger, D. *Phys. Rev. Appl.* **2017**, *7*, 024031.
(22) Koenderink, A. F. *ACS Photonics* **2017**, *4*, 710−722.
(23) Arcari, M.; Söllner, I.; Javadi, A.; Lindskov Hansen, S.; Mahmoodian, S.; Liu, J.; Thyrrestrup, H.; Lee, E. H.; Song, J. D.; Stobbe, S.; et al. *Phys. Rev. Lett.* **2014**, *113*, 1−5.
(24) Goban, A.; Hung, C.-L.; Hood, J. D.; Yu, S.-P.; Muniz, J. A.; Painter, O.; Kimble, H. J. *Phys. Rev. Lett.* **2015**, *115*, 063601.
(25) Shalaginov, M. Y.; Vorobyov, V. V.; Liu, J.; Ferrera, M.; Akimov, A. V.; Lagutchev, A.; Smolyaninov, A. N.; Klimov, V. V.; Irudayaraj, J.; Kildishev, A. V.; et al. *Laser Photon. Rev.* **2015**, *9*, 120−127.
(26) Lu, D.; Kan, J. J.; Fullerton, E. E.; Liu, Z. *Nat. Nanotechnol.* **2014**, *9*, 48−53.
(27) Sipahigil, A.; Evans, R. E.; Sukachev, D. D.; Burek, M. J.; Borregaard, J.; Bhaskar, M. K.; Nguyen, C. T.; Pacheco, J. L.; Atikian, H. A.; Meuwly, C.; et al. *Science* **2016**, *354*, 847−850.
(28) Bozhevolnyi, S. I.; Khurgin, J. *Optica* **2016**, *3*, 1418−1421.
(29) Yang, J.; Faggiani, R. M.; Lalanne, P. *Nanoscale Horiz. Nanoscale Horiz* **2016**, *1*, 11−13.
(30) Kongsuwan, N.; Demetriadou, A.; Chikkaraddy, R.; Benz, F.; Turek, V. A.; Keyser, U. F.; Baumberg, J. J.; Hess, O. *ACS Photonics* **2018**, *5*, 186−191.
(31) Moreau, A.; Ciracì, C.; Mock, J. J.; Hill, R. T.; Wang, Q.; Wiley, B. J.; Chilkoti, A.; Smith, D. R. *Nature* **2012**, *492*, 86−89.
(32) Faggiani, R.; Yang, J.; Lalanne, P. *ACS Photonics* **2015**, *2*, 1739−1744.
(33) Chikkaraddy, R.; de Nijs, B.; Benz, F.; Barrow, S. J.; Scherman, O. A.; Rosta, E.; Demetriadou, A.; Fox, P.; Hess, O.; Baumberg, J. J. *Nature* **2016**, *535*, 127−130.
(34) Akselrod, G. M.; Argyropoulos, C.; Hoang, T. B.; Ciracì, C.; Fang, C.; Huang, J.; Smith, D. R.; Mikkelsen, M. H. *Nat. Photonics* **2014**, *8*, 835−840.
(35) Hoang, T. B.; Akselrod, G. M.; Argyropoulos, C.; Huang, J.; Smith, D. R.; Mikkelsen, M. H. *Nat. Commun.* **2015**, *6*, 7788.
(36) Hoang, T. B.; Akselrod, G. M.; Mikkelsen, M. H. *Nano Lett.* **2016**, *16*, 270−275.
(37) Doherty, M. W.; Manson, N. B.; Delaney, P.; Jelezko, F.; Wrachtrup, J.; Hollenberg, L. C. L. *Phys. Rep.* **2013**, *528*, 1−45.
(38) Mock, J. J.; Hill, R. T.; Degiron, A.; Zauscher, S.; Chilkoti, A.; Smith, D. R. *Nano Lett.* **2008**, *8*, 2245−2252.
(39) Mertens, J.; Kleemann, M.-E.; Chikkaraddy, R.; Narang, P.; Baumberg, J. J. *Nano Lett.* **2017**, *17*, 2568−2574.
(40) Aslam, N.; Waldherr, G.; Neumann, P.; Jelezko, F.; Wrachtrup, J. *New J. Phys.* **2013**, *15*, 13064.
(41) Choy, J. T.; Hausmann, B. J. M.; Babinec, T. M.; Bulu, I.; Khan, M.; Maletinsky, P.; Yacoby, A.; Lončar, M. *Nat. Photonics* **2011**, *5*, 738−743.
(42) Liebermeister, L.; Petersen, F.; Münchow, A. v.; Burchardt, D.; Hermelbracht, J.; Tashima, T.; Schell, A. W.; Benson, O.; Meinhardt, T.; Krueger, A.; et al. *Appl. Phys. Lett.* **2014**, *104*, 031101.
(43) Mohtashami, A.; Femius Koenderink, A. *New J. Phys.* **2013**, *15*, 43017.
(44) Lassiter, J. B.; McGuire, F.; Mock, J. J.; Ciracì, C.; Hill, R. T.; Wiley, B. J.; Chilkoti, A.; Smith, D. R. *Nano Lett.* **2013**, *13*, 5866−5872.
(45) Akselrod, G. M.; Ming, T.; Argyropoulos, C.; Hoang, T. B.; Lin, Y.; Ling, X.; Smith, D. R.; Kong, J.; Mikkelsen, M. H. *Nano Lett.* **2015**, *15*, 3578−3584.
(46) Andersen, S. K. H.; Kumar, S.; Bozhevolnyi, S. I. *Nano Lett.* **2017**, *17*, 3889−3895.
(47) Bahari, B.; Tellez-Limon, R.; Kante, B. *J. Appl. Phys.* **2016**, *120*, 93106.
(48) Kinkhabwala, A.; Yu, Z.; Fan, S.; Avlasevich, Y.; Müllen, K.; Moerner, W. E. *Nat. Photonics* **2009**, *3*, 654−657.
(49) Nicolodi, D.; Argence, B.; Zhang, W.; Le Targat, R.; Santarelli, G.; Le Coq, Y. *Nat. Photonics* **2014**, *8*, 219−223.
(50) Rondin, L.; Tetienne, J. P.; Hingant, T.; Roch, J. F.; Maletinsky, P.; Jacques, V. *Rep. Prog. Phys.* **2014**, *77*, 56503.
(51) O'Brien, J. L.; Furusawa, A.; Vučković, J. *Nat. Photonics* **2009**, *3*, 687−695.
(52) Piatkowski, L.; Accanto, N.; van Hulst, N. F. *ACS Photonics* **2016**, *3*, 1401−1414.
(53) Benz, F.; Schmidt, M. K.; Dreismann, A.; Chikkaraddy, R.; Zhang, Y.; Demetriadou, A.; Carnegie, C.; Ohadi, H.; de Nijs, B.; Esteban, R.; et al. *Science* **2016**, *354*, 726−729.

DOI: 10.1021/acs.nanolett.8b01415
Nano Lett. XXXX, XXX, XXX−XXX

(54) Rivera, N.; Kaminer, I.; Zhen, B.; Joannopoulos, J. D.; Soljačić, M. *Science* **2016**, *353*, 263−269.
(55) Lovchinsky, I.; Sushkov, A. O.; Urbach, E.; de Leon, N. P.; Choi, S.; De Greve, K.; Evans, R.; Gertner, R.; Bersin, E.; Muller, C.; et al. *Science* **2016**, *351*, 836−841.
(56) Schwartz, I.; Cogan, D.; Schmidgall, E. R.; Don, Y.; Gantz, L.; Kenneth, O.; Lindner, N. H.; Gershoni, D. *Science* **2016**, *354*, 434−437.

DOI: 10.1021/acs.nanolett.8b01415
Nano Lett. XXXX, XXX, XXX−XXX